Elsevier Editorial System(tm) for Remote Sensing of Environment
Manuscript Draft

Manuscript Number: RSE-D-10-00815

Title: Remote sensing of the Caspian Sea level changes using decadal TOPEX/Poseidon altimetry data.

Article Type: Full length article

Keywords: Caspian Sea level, water resource, TOPEX/Poseidon, water management, least squares spectral analysis (LSSA).

Corresponding Author: Mr Ehsan Forootan,

Corresponding Author's Institution: Bonn University

First Author: Mohamad. A. Sharifi, Dr

Order of Authors: Mohamad. A. Sharifi, Dr; Ehsan Forootan; Mehdi Nikkhoo; Joseph. L. Awange, Dr; Mehdi Najafi-Alamdari, Professor

Reasearch highlights:

- 1. Decadal process of the TOPEX/Poseidon (T/P) satellite altimetry data set over the Caspian Sea.
- 2. Presenting the point-wise and pass-wise approaches to monitor an inland water body such as the Caspian Sea using satellite altimetry observations.
- 3. Presenting the least squares spectral analysis approach as a reliable tool to analyze the sea level variations.
- 4. Compute the tidal and the T/P's orbital frequencies within the Caspian Sea.
- 5. Discovering the influence of the Volga River's frequencies on the level variations of the Caspian Sea.

Remote sensing of the Caspian Sea level changes using decadal TOPEX/Poseidon altimetry data.

M. A. Sharifi[a], E. Forootan[b], M. Nikkhoo[c], J. L. Awange[d,e], M. Najafi-Alamdari[f]

[a] *Surveying and Geomatics Engineering Department, University of Tehran, Iran*
[b] *Institute of Geodesy and Geoinformation (IGG), Bonn University, Bonn, Germany*
[c] *Geodesy and Geomatics Engineering Department, K.N. Toosi University of Technology, Iran*
[d] *Western Australian Centre for Geodesy and The Institute for Geoscience Research Curtin University, Perth, Australia*
[e] *Geodetic Institute, Karlsruhe Institute of Technology (KIT), Karlsruhe, Germany*
[f] *Geodesy and Geomatics Engineering Department, K.N. Toosi University of Technology, Iran*

Abstract

The Caspian Sea is an economical resource, that supports the population of five countries (Iran, Russia, Kazakhstan, Turkmenistan and Azerbaijan), and regulates the region's climate. It has displayed considerable fluctuations in its water level during the past few years, necessitating its monitoring. Knowledge of such fluctuation is vital for understanding the local hydrological cycle, the region's climate, supporting flood management plans, and construction activities within the sea and along its shore-lines. The average water level variation of the Caspian Sea, is however, rather complicated and non-periodic as indicated by long-term space-borne and terrestrial records. These variations have been mostly influenced by changes in water inflow rates due to changes in the agricultural policies of neighboring countries. The aim

Email address: forootan@geod.uni-bonn.de (E. Forootan)

of this paper is to evaluate the temporal variations in the level of the Caspian Sea using 400 cycles of the complete TOPEX/Poseidon satellite altimetry data for the period 1993 to 2003. Use is also made of the Anzali Port tide gauge data for the period 1982 to 2003, and 5 years of monthly discharge data from the river Volga. The study employs least squares spectral analysis (LSSA) to find the most significant frequencies and the mean value of the observed variations. The results indicate a long-term (12.5-years period) and that on average, the Caspian Sea's level rose at a rate of about 15 cm/year from 1993 to 1995, while from 1995 to 2003, there was an average decline of nearly 6 cm/year. Cross-correlation of the Volga's power spectrum with the powers of the northern-most, middle and southern-most points within the Caspian Sea were respectively 0.63, 0.51 and 0.4 of zero-lag correlation, indicating the influence of Volga River on the level of the Caspian Sea, which may be useful for further predictions. Comparing point-wise and pass-wise modes of fluctuation analysis, our results show that the point-wise approach could be the most suitable method for the preliminary monitoring of this inland water resource as it gives accurate local fluctuations that are not visible in pass-wise analyses.

Keywords: Caspian Sea level, water resource, TOPEX/Poseidon, water management, least squares spectral analysis.

1. Introduction

The Caspian Sea (Fig. 1), situated between latitudes 37°N and 47°N and longitudes 45°E and 54°E is the world's largest inland water body with an area of about 400,000 km^2, stretching approximately 1,200 km long in the

north-south direction (e.g., Dumont (1998); Rodionov (1994)). Its width ranges from 435 km to a minimum of 196 km, while its length is divided into three sub-basins (the most northern, the middle, and the southern parts). Most of the northern Caspian is shallow, with an average depth of 4 m. The average depth increases southwards with it being about 800 m around the central and approximately 1 km in the southern Caspian (Dumont et al. (2004)). The Caspian Sea has no connection to the world's oceans and its surface level is around -26.5 m below Mean Sea Level (MSL).

Economically, it is vital for sturgeon production, oil and gas resources (e.g., Dumont (1998)). The variability in salinity, depth, and climate over the sub-basins give it a unique attribute compared to other major inland water bodies, such as Lake Victoria in East Africa (e.g., Awange & Ong'ang'a (2006)). For instance, Dumont (1998) states that within these three sub-basins, the north behaves like a temperate shallow lake, the central a climatic basin, and the south a meromictic lake (i.e., with layers of water that do not mix), comparable to the Black Sea.

However, the Caspian Sea displayed considerable fluctuations in its water levels, which have been the subject to several studies (e.g., Rodionov (1994); Kosarev & Yablonskaya (1994); Swenson & Wahr (2007)). Ignatov et al. (1993), for example, explained the cause of these fluctuations to be possibly climatic, and that it is dependent on the water budget of its basin (precipitation and river discharge minus water loss by evaporation). Short-term wind-induced fluctuations are known to cause a rise of up to 4 m, although the average fluctuation is about one meter. Other causes include barometric pressure, tidal variations (often less than 1 m), and seasonal rises induced

by high rates of water flow during spring water in the rivers (lesser effect). Indeed, fluctuations of inland water bodies are sensitive to climate change and serve as one of its indicators, as was demonstrated in the case of Lake Victoria in East Africa, e.g., by Awange et al. (2008).

On the one hand, the Caspian Sea level changes play a vital role in indicating regional climate change given its three micro-climatic basins. Its flooding on the other hand could lead to environmental and economic damage as was the case following its sudden rise in 1978 (Ignatov et al. (1993); Cazenave et al. (1997)). Moreover, Caspian Sea fluctuations have been shown, e.g., by Leontiev et al. (1997, in Ignatov et al. 1993) to be cyclic over 30-50 years, thereby prompting Ignatov et al. (1993) to warn that if the cyclic pattern is true, a further rise of its water level should be expected in the near future. Knowledge of the fluctuation of its water level, therefore, is not only vital as an indicator of the changing climate, but also to inform environmental flood management programs, thus necessitating the need for continuous monitoring of variations in its level.

Long-term (century-scale) fluctuations of Caspian Sea have been reconstructed from archaeological, geographical, and historical data. The task has been compounded by its sheer size, which makes determining its average water level more complicated. Long-term records show that the average level has varied considerably over the last fifty years, and many studies have been undertaken to attempt to predict mean water-level variations (e.g., Georgievskiy (2001, and references therein)). Monitoring variations in the water level of inland water bodies the size of the Caspian Sea requires an accuracy and completeness of geographical data coverage that challenges

conventional measurement capabilities such as tide gauges.

To meet this challenge, in recent years, space-based remote sensing has provided essential new information. One example is the TOPEX/Poseidon (T/P) mission, a satellite altimetry approach which was designed to precisely monitor absolute sea level variations (e.g., Minster et al. (1995); Nerem (1995)), but also found application in monitoring inland lake level changes (e.g., Birkett (1994, 1995)). T/P was applied, e.g., by Cazenave et al. (1997) to monitor the Caspian Sea level from January 1993 until August 1996 (i.e., 3.5 years), from which a fall in its level was shown. Kostianoy & Lebedev (2006) studied the level fluctuation using nine points located on the T/P's cross-tracks. Swenson & Wahr (2007) used a different satellite altimetry, Jason, together with the GRACE (Gravity Recovery And Climate Experiment) products to analyze the water storage variation of the Caspian Sea from mid 2002 to 2006, and provided a means by which indirect satellite data could be validated.

In this study, we extend the previous work of Cazenave et al. (1997) and Kostianoy & Lebedev (2006) by employing a complete dataset of the T/P mission spanning a decade from 1993 to 2003 to monitor temporal variations of the Caspian Sea level with the aim of analyzing the characteristics of its frequencies. To achieve this, the study consist of the following parts:

(1) Pass-wise analysis to obtain a synthesis of the Caspian water level changes and a global impact of its variations.

(2) Least Squares Spectral Analysis (LSSA) of point-wise Sea Surface Height (SSH) residuals' time-series to detect the significant frequencies of variability. This is achieved through (i) generating point-wise time-series

from T/P repeated cycles located within the Caspian Sea (over 260 time series with reliable observations are generated), (ii) trend analysis of the over 30 years (1982 to 2006) in-situ tide gauge data of Anzali port to establish a suitable trend of the Caspian Sea's water level, (iii) analysis of the residual observations to detect available minor frequencies, (iv) analysis of the T/P satellite's orbital frequencies in order to point out the interfering frequencies in the SSH time-series, and (v) analysis of the Volga River discharge in order to show its correlation with the Caspian Sea's level fluctuations using 5 years monthly Volga discharge data.

In the next section, we briefly describe the Caspian Sea. The data used in the study is presented in Section 3, while Section 4 outlines the analysis methods, and the results presented and discussed in Section 5. Finally, Section 6 summarizes the major findings.

2. The Caspian Sea

Caspian Sea (Fig. 1) is supplied mainly by discharge from rivers and precipitation. Its water budget is completed by being drained predominantly through evaporation and a minor outlet to Kara-Bobaz Gulf. The largest of these rivers is the Volga, which drains an area of 1,400,000 km^2 and runs into the north-western part of the Caspian, contributing more than 80% of the total inflow (Dumont (1998)). The Volga River, together with Kura, Terek, Ural and Sulak, supply over 90% of the inflowing freshwater to the Caspian Sea. The Iranian rivers and smaller streams on the north-eastern part of the country supply the remaining 10%, since there are no permanent inflows on

the eastern side (e.g., Kazakhstan and Turkmenistan regions) (TDA (2002)).

The Sea's salinity averages about 12.8 psu, which is almost three times lower than what is normally found in the open oceans, especially in the northern Caspian, where there is a large inflow of fresh water from the Volga and Ural rivers. Ice forms in the northern portions of the Caspian in early November and reaches its maximum southern extent by January or February (Kosarev & Yablonskaya (1994)).

The climatic conditions of the Caspian Sea are influenced by cold Arctic air, moist sea air masses forming over the Atlantic ocean, dry continental air masses from Kazakhstan, and warm air masses coming from the Mediterranean Sea and Iran. According to Rodionov (1994), three types of the atmospheric circulation over Russia exist. Among them, the meridian type, which is characterized by stable high pressure over European Russia, resulting in cold winters and hot cloudless summers, is most common and has been more dominant than usual over the Caspian Sea in recent years.

Extreme temperature conditions contribute to the changing Caspian Sea level. In most locations, general tides, surges and waves combine to define the maximum conditions of the water levels. Since tides and storms and related surges and waves differ in nature, a probabilistic approach including combined statistics of tides and storms, has been used to monitor the variations (von Storch & Woth (2008)). Studies (e.g. Ignatov et al. (1993); Cazenave et al. (1997)) show that, the largest uncertainty for the Caspian Sea is that of its average water level, which by itself is not subject to a statistical distribution, but is rather more related to a trend. Hence, combining joint probability analysis of the parameters is not possible. It appears that

the very large variations in its water level are due to natural oscillations of various components that make up the region's water balance.

FIGURE 1

3. Data

Three datasets were used in this study. These are (i) derived water levels from T/P satellite altimetry mission, (ii) water levels from tide gauge in-situ measurements provided by the Iranian Caspian Environmental Study Center, and (iii) 5 years Volga River monthly discharge data.

The altimetry data are processed at the Jet Propulsion Laboratory (JPL), USA and cover repeated T/P mission cycles 11 to 400, spanning more than 10 years. The T/P mission has offered a great potential with an accuracy of 4 cm having so far been achieved for inland seas, lakes and reservoirs (see e.g., Birkett (1995); Hwang et al. (2005); Medina et al. (2008)).

3.1. TOPEX/Poseidon (T/P) altimetry data

The launching of the T/P mission on 10th August 1992 opened a new era for understanding global ocean dynamics by making precise and accurate observations of sea-level variation. The satellite covers the Earth from 66 °N to 66 °S which includes most of the ice-free oceans. The T/P satellite orbited at an altitude of 1,336 km above the reference ellipsoid (a mathematical figure approximating the mean sea level) and measured the distance between the satellite and the Earth's sea surface with an accuracy of 4 cm (e.g., Birkett (1995)). Each T/P cycle includes 254 passes, where 127 are ascending and 127

descending. In most of them, eight ground tracks pass through the Caspian Sea with reliable altimetry, as shown in Fig. (1).

To obtain the SSH of the Caspian Sea during the more than ten years of our study period (1993-2003), the entire dataset obtained from the beginning of the T/P mission to the 400th cycle in the form of *Merged Geophysical Data Record* (MGDR) are used. Since cycles 1 to 10 do not contain reliable information, as such, they are omitted and the analysis is carried out from the 11th cycle, which has adequate data as a reference cycle.

In general, each MGDR file incorporates improved orbits (e.g., Nerem et al. (1993)) that yield satellite heights from a reference ellipsoid. The main data of the MGDR is the altimetric ranges measured at the Ku and C bands. In this study, the Ku band range data are used, which is recommended for most applications (e.g., Benada (1997)). The range provided in MGDR are already corrected for instrumental effects such as drifts. However, it must be corrected for the atmospheric errors (e.g., ionospheric and tropospheric effects), which affect the radar pulse as it passes through the atmosphere, and the nature of the reflecting sea surface. The corrected range is calculated from the following equation (Benada (1997)):

$$\rho^{\mathrm{c}} = \rho + \Delta w + \Delta d + \Delta I + \Delta IB + \Delta E + \Delta PT + \Delta CM, \qquad (1)$$

where ρ^{c} and ρ are the corrected and measured range values respectively, Δw, Δd and ΔI are the wet troposphere, dry troposphere and ionosphere corrections, respectively. Electromagnetic bias and inverse barometer errors are corrected by the terms ΔE and ΔIB, respectively. Corrections due to temporal variations in the used coordinate system, i.e., the geocentric pole

tide and center of gravity motions, are given by the terms ΔPT and ΔCM, respectively. All of the correction parameters in Eq. (1) are included in the provided MGDR data, and were used to correct the measured ranges.

Since this study aims at monitoring the instantaneous sea level and determine the significant frequencies using the point-wise approach discussed in Section. 5.2, we did not correct the data for tidal effects. However, the tidal coefficients are derived from LSSA once each time series has been computed and used to compute tidal frequencies that are removed. Once the data has been corrected according to Eq. (1), the instantaneous ellipsoidal height of sea surface (SSH) is computed by the difference:

$$\mathrm{SSH}(\phi, \lambda, t) = H_{\mathrm{sat}}(\phi, \lambda, t) - \rho^{\mathrm{c}}(\phi, \lambda, t), \tag{2}$$

where $H_{\mathrm{sat}}(\phi, \lambda, t)$ is the altitude of the satellite at a given location and time measured from the reference ellipsoid provided in MGDR dataset.

3.2. Tide-gauge data

This study used daily tide gauge records of the Anzali port tide gauge station (Fig. 1) from 1982 to 2007 to find the long-term trend of the level variations in the Caspian Sea. Then this trend is used for detrending the SSH data. Sea-level recording has a relatively long history in Bandar-e Anzali (a harbour town on the Caspian Sea, in the Iranian province of Gilan). The Anzali tide gauge is one of the stations with quite a long time series, being carried out for the past 50 years on a daily basis (Bird (2010)). The gauge station is located in the south-eastern part of the Caspian Sea at 37.47 °N and 49.46 °E. Tide-gauge data records have been widely used to monitor sea level

changes (Gil & de Toro (2005)). Gil & de Toro (2005) states that recording sea-level changes at a fixed location for a suitable period of time can be used to determine the sea surface harmonic oscillation generated by harmonic forces via the harmonic analysis scheme. Therefore, obtaining frequencies from gauge observations is also a reliable method of evaluating the frequencies resulting from the spectral analysis of space-borne sea surface height (SSH).

3.3. Volga River data

Traditionally, the Volga River basin is subdivided into three parts according to the general climatic background characteristics: northern (from northern margins down to approximately the latitude of Saratov), the central or middle part of the basin (approximately from Saratov to Volgograd) and the southern (approximately from Volgograd to southern margins along the Caspian Sea shores and the Kazakhstan border) (Golosov & Belyaev (2010)). Since the discharge of the southern basin directly affects the sea level of Caspian, here, we used the available monthly discharge data from 1999 to 2005 measured at the Volgograd hydro-electric power station located upstream from where the Volga flows into the Caspian Sea (Fig. 1).

4. Analysis

4.1. Time-series spectral analysis

Spectral analysis is a method of function approximation, which can be used to describe natural phenomena. Choosing a suitable norm and base functions in a vector space is essential for the appropriate approximation of a random function's behavior. Any priori information dealing with the physical behavior of a measured observable should be incorporated in selecting the

base functions (Vanícêk & Krakiwsky (1986)). Sine and cosine base functions, therefore, are well-suited for modeling sea surface variations due to the periodic behavior of the sea surface height variations (e.g. Foster (1996)).

The least squares estimation technique is frequently used for deterministic modeling of measurements (Vanícêk (1969)). For a periodic observable, the deterministic part consists of a limited number of periodic components. The least squares estimation is employed to decompose any measured observable to its components which is equivalent to traditional power spectral density determination methods (e.g., Fourier analysis). However, the traditional methods are significantly limited in their applications. They always require equally spaced data in the argument, which is the most seldom case in practice since, observations are usually unequally spaced and scattered (e.g., Vityazev (1996); Rubin (2002)). Therefore, the unequally spaced original data should be mapped to an equidistant grid. Depending on the smoothness of the original series, the presence of data gaps, and the subjective choice of the mapping function, a new set of observations are generated. The problem is even more critical if one maps the data by interpolation schemes, which also tend to smooth out any high frequency components of the original data series. To overcome these limitations and difficulties, Vanícêk (1969) developed a method of spectrum computation on the basis of least squares estimation. The method, known as *Least Squares Spectral Analysis (LSSA)*, has been widely applied in geosciences (e.g., Wu et al. (1995); Craymer (1998)).

In the method of spectral analysis, measurements are assumed as a vector in a Hilbert space. At each step, the orthogonal projection of an $n \times 1$

observation vector $\mathbf{f}$ onto an m-dimensional subspace $\mathbb{S}$, spanned by m base functions, is obtained by (Vanícêk (1969)):

$$\mathbf{p} = \sum_{i=1}^{m} c_i \phi_i, \tag{3}$$

where c_i are unknown coefficients of the linear combination in terms of the basis ϕ_i given in Eq. 5. In vector and matrix notation, the representation in Eq. 3 becomes

$$\mathbf{p} = \mathbf{c}\boldsymbol{\phi}, \tag{4}$$

where c_i and ϕ_i are the entries of the column vector $\mathbf{c}$ and the matrix $\boldsymbol{\phi}$ respectively. The least squares estimation of the unknown coefficients are therefore given by

$$\hat{\mathbf{c}} = (\boldsymbol{\phi}^T \boldsymbol{\phi})^{-1} \boldsymbol{\phi}^T \mathbf{f}, \tag{5}$$

where $\mathbf{f}$ is the vector of observations, here, the sea surface heights from T/P or tide gauge measurements. Inserting the estimated coefficients $\hat{c}_i$ from Eq. (5) into Eq. (3) gives the orthogonal projection of the observation vector $\mathbf{f}$ onto subspace $\mathbb{S}$. Spectral values are computed by performing a second orthogonal projection of $\mathbf{p}$ back onto $\mathbf{f}$ (Fig. 2).

FIGURE 2

Back-projection of $\mathbf{p}$ onto $\mathbf{f}$ gives the contribution of subspace $\mathbb{S}$ to the observations and is obtained by

$$\frac{\langle \mathbf{f}.\mathbf{p} \rangle}{\| \mathbf{f} \|}, \tag{6}$$

where $\langle \mathbf{f}.\mathbf{p} \rangle$ is the inner product and $\| \mathbf{f} \|$ the length of vector $\mathbf{f}$. This ratio, therefore, is defied as the *spectral value* (e.g., Vanícêk (1969)), given by

$$S(\omega) = \frac{\langle \mathbf{f}.\mathbf{p} \rangle}{\langle \mathbf{f}.\mathbf{f} \rangle}. \tag{7}$$

S may be described as the amount of the vector $\mathbf{f}$ contained in subspace $\mathbb{S}$. This value varies between zero and one, which indicates that the observation vector is orthogonal to the subspace or completely belongs to it, respectively (Wells et al. (1985)).

4.2. Least Square Spectral Analysis (LSSA)

Consider a set of real and positive frequencies $\{\omega_1, \omega_2, \cdots, \omega_m\}$, whose spectral values for a given observation vector are to be determined. For each frequency ω_i, $\boldsymbol{\phi}^{\mathrm{c}}(\omega_i)$ and $\boldsymbol{\phi}^{\mathrm{s}}(\omega_i)$ are defined as the base functions of the corresponding subspace

$$\boldsymbol{\phi}^{\mathrm{c}}(\omega_i) = \begin{pmatrix} \cos\omega_i t_1 & \cos\omega_i t_2 & \cdots & \cos\omega_i t_n \end{pmatrix}^T \tag{8}$$

$$\boldsymbol{\phi}^{\mathrm{s}}(\omega_i) = \begin{pmatrix} \sin\omega_i t_1 & \sin\omega_i t_2 & \cdots & \sin\omega_i t_n \end{pmatrix}^T, \tag{9}$$

where $t_1, t_2, \cdots, t_n$ are the observations times, and could be either equally or unequally spaced measurement epochs. The vectors $\boldsymbol{\phi}^{\mathrm{c}}(\omega_i)$ and $\boldsymbol{\phi}^{\mathrm{s}}(\omega_i)$ construct a design matrix $\boldsymbol{\phi}(\omega_i) = [\boldsymbol{\phi}^{\mathrm{c}}(\omega_i)\ \boldsymbol{\phi}^{\mathrm{s}}(\omega_i)]$. Multiplying Eq. (5) by $\boldsymbol{\phi}(\omega_i)$ leads to

$$\hat{\mathbf{c}}\boldsymbol{\phi}(\omega_i) = \boldsymbol{\phi}(\omega_i)(\boldsymbol{\phi}^T\boldsymbol{\phi})^{-1}\boldsymbol{\phi}^T\mathbf{f}, \tag{10}$$

whose left hand side is $\mathbf{p}(\omega_i)$ in Eq. (4). Replacing $\mathbf{p}(\omega_i)$ in Eq. (7) leads to spectral value corresponding to ω_i,

$$S(\omega_i) = \frac{\mathbf{f}^T\mathbf{p}(\omega_i)}{\mathbf{f}^T\mathbf{f}} = \frac{\mathbf{f}^T\boldsymbol{\phi}(\omega_i)(\boldsymbol{\phi}^T(\omega_i)\boldsymbol{\phi}(\omega_i))^{-1}\boldsymbol{\phi}^T(\omega_i)\mathbf{f}}{\mathbf{f}^T\mathbf{f}}. \tag{11}$$

The set of all these spectral values for all frequencies is called the *least squares spectrum* of the observation vector $\mathbf{f}$,

$$\mathbf{s}(\boldsymbol{\omega}) = \{S(\omega_1), S(\omega_1), \cdots S(\omega_m)\}. \tag{12}$$

It is necessary to remark that if ω_i is equal to zero, the vector of $\boldsymbol{\phi}^{\mathrm{s}}(\omega_i)$ will also be equal to zero. Thus, it is not a base function of subspace $\mathbb{S}$ and will be omitted from $\boldsymbol{\phi}(\omega_i)$. In this case, $\hat{\mathbf{c}}$ is replaced by a scalar whose estimated value is the mean value of observations.

4.3. Statistical test

The significance of the estimated spectral values can be tested statistically, thus providing one of the main advantages of the least squares spectral analysis. Steeves (1981) showed that the criteria for accepting or rejecting the null hypothesis, $H_0 : S(\omega_i) = 0$, is defined as:

$$S(\omega_i) = \begin{cases} \leq \left(1 + \frac{\nu}{2}F_{\nu,2,\alpha}\right)^{-1} & ; \quad \text{Accept } H_0 \\ \\ > \left(1 + \frac{\nu}{2}F_{\nu,2,\alpha}\right)^{-1} & ; \quad \text{Reject } H_0, \end{cases} \tag{13}$$

where $F_{\nu,2,\alpha}$ is the critical value of Fisher distribution with ν and 2 degrees of freedom at a significance level of $1-\alpha$. The results of the statistical tests provided in this study correspond to a 95% level of confidence ($\alpha = 0.05$).

4.4. Aliasing phenomenon

According to the Nyquist-Shannon sampling theorem (Shannon (1984)), the maximum detectable frequency of a continuous function, which is sampled equidistantly in n points with spacing Δt, is

$$\nu_{\max} = \frac{1}{2\Delta t} = \frac{n}{2T} = \frac{n}{2}\nu_0, \tag{14}$$

where $T = t_n - t_1$ and ν_0 are the length of the observation time-series and the fundamental or natural frequency, respectively, and $\nu_{\max}$ is the Nyquist frequency (e.g., Awange et al. (2008)).

A continuous time series can only be completely reconstructed from sampled values if the sampling time interval is smaller than $\frac{1}{2\nu_{\max}}$. Otherwise, the period of the component of signal with a frequency of ν aliases to ν_{a}. Therefore, for T/P satellite altimeter data with a temporal resolution of 9.915625 days, some of the tidal frequencies with periods less than 10 days will be aliased. According to Wang (2004), for an actual tidal frequency ν^k, there is an aliased frequency ν_{a}^k such that

$$\nu_{\mathrm{a}}^k = |\mathrm{mod}\left(\nu^k + \frac{\nu_{\mathrm{s}}}{2}, \nu_{\mathrm{s}}\right) - \frac{\nu_{\mathrm{s}}}{2}|, \tag{15}$$

where ν_{s} is the sampling frequency of satellite altimetry. The length of the observation vector should be long enough so that two close tidal components, ν_1 and ν_2 can be separated. This involves determining the Raylight period T_{r} which is defined as,

$$T_{\mathrm{r}} = |\frac{\nu_1}{2\pi} - \frac{\nu_2}{2\pi}|, \tag{16}$$

where π is equal to 3.14 and ν_1 and ν_2 are two neighboring frequencies. In order to separate the ν_1 and ν_2, observation period should be larger than the Raylight period. Consequently, we are able to determine all the main tidal frequencies (except the 18.6 years of the moon) using 3 years of T/P observations. Moreover, two marginal Sun semidiurnal and Sun semiannual frequencies are able to be separated if we use 9 years of T/P observations. Therefore, we could expect to sense nearly all tidal components using a decade $(1993 - 2003)$ of satellite altimetry data (cf. Wang (2004)).

5. Results and Discussion

5.1. Pass-wise analysis

Figure (1, red lines) shows that nearly seven (out of 254) T/P passes cross the Caspian Sea. Since each ground track of the T/P satellite tacks less than a few minutes to cross the Caspian Sea and also due to negligible tidal influence within a few minutes, all observations from each pass can be assumed to have been observed simultaneously. One can then obtain a good estimate of the mean sea level by computing the mean value of each of these passes. In this study, we call this method the *pass-wise approach*. To obtain a better estimation, we have considered all available data from the main six passes (16, 31, 57, 92, 133, 168) to infer Caspian Sea water-level changes (see Figs. 1 and 3).

Figure 3 shows the mean values of these six passes during the observation period $(1993 - 2003)$, which are interpolated to monthly time step. All passes generally show more or less identical pattern in the sea level variations. From 1993 until 1995, the sea experienced a rise, after which it shows a

declined from 1995 to 2003. Despite the similarity in the whole sea level variations, different fluctuations are observed at different locations. Due to these difference, a least squares linear regression is employed to derive the rate of mean water-level variation for each pass. The linear regression is shown by the solid red lines in Fig. 3. On average, the water level rose at a rate of about 15 cm/year between 1993 to 1995, whereas the average declining rate was nearly 6 cm/year between 1995 to 2003.

FIGURE 3

5.2. Point-wise analysis

The sea level variations can also be viewed from another perspective. The satellite's footprints from different cycles are located in close proximity since the T/P satellite orbits the Earth in a repeat mode. Consequently, one can interpret each altimetry point as a virtual tide gauge where the sea surface height is observed every 9.915625 days. From this perspective, satellite observed sea heights can be independently analyzed for each observation location.

However, T/P does not repeat exactly at the same ground track. Differences between tracks are around 1 km (e.g., Hwang et al. (2005)). Therefore, it is necessary to map repeated sea level observations of different cycles to a reference cycle. While the separation between every two sequential measurements in one pass is around 5 km, we treat all the observations from *cycle* 011 as the reference points. Then, those observations from other cycles that are located within a radius of 3 km to the reference points are considered repeated observations. However, the definition of the detected points

as time series introduces a problem, that is different cycles have a different geoid profile. This effect is called the cross-track geoid gradient and has a non-negligible influence on SSH (Benada (1997)). The problem is solved by reducing the SSH of the detected points by the geoid difference to the reference point. Using the *point-wise approach*, 260 time series with reliable records are computed over three points in the Caspian Sea (i.e., the northern-most, middle, and southern-most points in Fig. 1). Figure 4 shows a sample time series computed for the middle point in the Caspian Sea.

FIGURE 4

It is necessary to mention that the computed time series in the point-wise approach depicts the behavior of sea level variations only at that single position and its surrounding and It cannot be generalized to other locations of the sea. Furthermore, due to the variations caused by external factors (e.g. the discharge of the Volga River in the north) every location experiences a different phase relationship. This will be discussed in details in Section. 5.5.

5.3. Trend analysis

Decomposition of the data series to the trends and residuals can be carried out only if the analytical model of the trend is stipulated. This means that the systematic behavior of the measurements is known with respect to the coordinates (in this case, time). It is necessary to remark that the term trend is loosely defined in this work as a long-term change in the mean level. A difficulty with this definition is deciding what is meant by a long-term, i.e., some climatic phenomena exhibit cyclic variations with a very long period.

Nevertheless, in the short term it may still be more meaningful to think of such a long-term oscillation as a trend. Chatfield (1989) defines trend as comprising all cycle components whose wavelength exceeds the length of observed time-series. This definition is adopted for our analysis.

Defining trend in the Caspian Sea is too complicated. Long-term in-situ observations in the Caspian Sea illustrate a nonlinear trend. However, Lyubushin et al. (2004), for example, considered a linear form to model the trend of Caspian Sea level variations before 1995. Based on the results of Figs. (3 and 4), however, it is clear that the behavior of the Caspian Sea water level has changed compared to the time before 1995.

The use of Bandar-e Anzali tide gauge records is therefore essential in establishing a nonlinear trend based on the least squares polynomial fit. The availability of daily records covering more than 30 years is the main reason for selecting this tide gauge for trend modeling (Fig. 5). Our analysis shows a polynomial function of degree six is suitable for modeling the trend. The order is evaluated by assessing the root mean square (RMS) of the residuals, and found that when increasing the order of the polynomial to higher than 6 did not decrease the RMS significantly. After trend removal, LSSA is implemented to the residuals using Eq. (11), which shows a 0.00022 cycle per day (cpd) frequency (≈ 12.5 years), compared to 12.8 years) found by (Lyubushin et al. (2004)).

FIGURE 5

The polynomial trend could only show the very low-frequency variations of sea level that are valid for points within the Caspian Sea. Thus, we will

use the estimated polynomial trend for detrending SSH observations before implementing LSSA (e.g., Fig. 5).

5.4. SSH frequencies

In the *point-wise approach*, the spectrum of every observed point independently shows the local sea surface behavior. However, the periodic components originate from common sources. Space-borne measured instantaneous sea surface height are the differences of satellite height and measured range (e.g., Eq. 2). Therefore, major periodic effects on SSH are due to;

- Seasonal and celestial tidal periodic effect on the measured range, or,
- Orbital periodic perturbations in the satellite position.

After removing the polynomial trend of the sample point height records, the residual observations are analyzed using LSSA (Eq. 11). The achieved results for the point which was shown in Fig. 4 are demonstrated in Fig. 6. The validity level is derived from implementing the statistical test (Eq. 13).

FIGURE 6

From the figure, tidal frequencies are clearly highlighted in the power spectrum of the signal. Of course, not all frequencies result from water level fluctuation. Due to the T/P's repeat frequency ($\nu_{\mathrm{s}} = 9.915965\,\mathrm{days}$), some aliased frequencies have emerged in the spectrum. For example, the aliased frequency of $\nu_{\mathrm{a}}^{\mathrm{M_2}} = 0.0161\,\mathrm{cpd}$ (≈ 62.107 days) is equivalent to the lunar semidiurnal frequency M_2 with $\nu^{\mathrm{M_2}} = 1.9305\,\mathrm{cpd}$. However, the other peaks, i.e., $\nu^{\mathrm{SA}} = 0.002738\,\mathrm{cpd}$ corresponds to the Sun annual frequency with a

period of 365.23 days. A summery of the major tidal frequencies and their computed aliased values corresponding to T/P sampling rate are listed in Table (1). The results are comparable with those of Eq. (14).

To explore the effect of non-tidal perturbation forces in the level variation signals, we corrected the time series for the seasonal and tidal periodic components. This was done by assuming the tidal frequencies listed in Table 1 as known, then their effects were computed from Eq. (11) and removed from the time series. As a result of this correction, short wavelength variations are superimposed on a long-term periodic fluctuation. In other words, the LSSA of the remaining part visualizes the unknown periodic constituents of the observed SSH if the omission error is neglected. For instance, Fig. 7 shows power spectrum of the sample point corresponding to Fig. 4 after removing the tidal components. A new peak that was already suppressed in total signal spectrum due to the significant effect of the tidal components emerges.

FIGURE 7

This new frequency is entered from the periodic perturbation of the satellite height since nearly all the periodic tidal components are removed from SSH. Spectral analysis of the residual orbital height, i.e., satellite altitude minus nominal orbital height minus tidal periodic effect, shows the same spectrum for the middle point in Fig. 1 (see Fig. 8A).

For the sake of completeness, the same analysis have been performed for two other satellite position above the Lake Victoria in East Africa (see the results in Fig. 8B) and the Atlantic ocean (in Fig. 8C). Their spectra are

Table 1: Main tidal components and their aliased frequencies. The first column indicates the sign of tidal frequencies, the second column the real value of the tidal frequencies derived from astronomical studies (c.f. Cartwright (1993)), the third column shows the corresponding real period, fourth column lists the computed frequencies with respect to T/P sampling rate, and the fifth column is their corresponding aliased periods.

Sign	Frequency (cpd)	Period (day)	Aliased Frequency (cpd)	Aliased Period (day)
SA	0.002738	365.260	0.002738	365.260
SSA	0.005476	182.621	0.005476	182.621
MSM	0.031435	31.812	0.031435	31.812
MM	0.036292	27.555	0.036292	27.555
MSF	0.067726	14.765	0.033125	30.189
MF	0.073202	13.661	0.027649	36.168
Q_1	0.893244	1.120	0.014417	69.365
O_1	0.929536	1.076	0.021875	45.714
P_1	0.997262	1.003	0.011250	88.891
S_1	1.000000	1.000	0.008512	117.485
K_1	1.002738	0.997	0.005774	17./192
O_2	1.859071	0.538	0.043750	22.857
N_2	1.895982	0.527	0.020191	49.528
M_2	1.932274	0.518	0.016101	62.107
S_2	2.000000	0.500	0.017024	58.742
K_2	2.005476	0.499	0.011548	86.596
M_3	2.898410	0.345	0.026274	38.061
M_4	3.864547	0.259	0.032202	31.054
S_4	4.000000	0.250	0.034047	29.371
M_6	5.796821	0.173	0.048303	20.702
S_6	6.000000	0.167	0.049780	20.088
M_8	7.729094	0.129	0.036447	27.437

similar to the spectrum of the middle point above the Caspian Sea. Of course, a few more meaningful components are visible in the lake Victoria spectrum whose detail interpretation is outside the scope of this paper.

FIGURE 8

5.5. Relationship to the Volga River

To study the influence of the Volga River on the water level variations of the Caspian Sea, we considered the three same points discussed previously (Fig. 1). The time series are derived from the *point-wise approach*, selected from the pass 92 (Fig. 1). Sea surface height power spectrum of these points are depicted in Fig. (9). The most northern point shows high fluctuations at high frequencies since the Caspian Sea is mostly fed by the Volga River discharge. The variations gradually changes to low-frequencies, which more or less show the local variations (see Fig. 9 and compare the amplitude of the peaks).

FIGURE 9

Analysis of the Volga River discharge could be very useful for classifying the peaks that appeared in the SSH spectrum in Fig. (9). The monthly record of the river outflow during $1999-2005$ is shown in Fig. (10C), with its power given in Fig. (10A). The spectrum shows the annual and semi annual frequencies are dominant in the discharge of Volga. Removing these two peaks leads to an amplification of less prominent components Fig. (10B). After removing the annual and semiannual peaks, the frequencies of 0.0068 cycle

per day (cpd), 0.0078 cpd, 0.0098 cpd and 0.0112 cpd emerge as the four significant peaks in Fig. (10B).

FIGURE 10

One can see that the SSH spectrum of the most northern point (Fig. 9A)is very similar to Volga discharge spectrum (Fig. 10B). Furthermore, it is clearly seen that the fluctuation of the sea surface in the north has short period. However, the middle and southern parts of the sea experience the longer-period effects of the Volga River (Fig. 9B and C). This is also confirmed from the computed cross-correlation of the Volga's power spectrum with the powers of Fig. 9. The results indicate 0.63, 0.51 and 0.4 of zero-lag correlation for the north, middle, and southern points, respectively.

To illustrate the effect of the Volga River on the Caspian Sea fluctuations, we computed the phase lag of the Volga's significant frequencies (Fig. 10B) from the sea surface height time series as a function of distance from the north (Volga entrance). The results are plotted in Fig. 11. The penetration of the first three frequencies (0.00068, 0.0078 and 0.0098 (cpd)) appears to vary southwards, whereas the phase lag of the 0.0112 cpd signal (Fig. 11D) is nearly constant in the same direction. Therefore, different locations experience the effect of the first three frequencies with a time delay, while the last component (0.0112 cpd) is visible simultaneously at different locations.

FIGURE 11

6. Conclusions

In this paper, we studied the spatial and temporal variations of the Caspian Sea's water level using T/P altimetry measurements. Our results show the major impact of the Volga River's discharge on the Caspian Sea level variation. Moreover, comparing pass-wise versus point-wise, our analysis demonstrates the superiority of the point-wise analysis for this case study while the sea level doest not change homogeneously within the water body. This is proved with implementing the LSSA to the time series of different locations of the sea which identified the different frequency structure of the fluctuations. A summary of the outcomes of this research are as follows:

- Analysis of pass-wise time-series shows a phase differences between various passes. It seems that these differences are due to the distance of the passes to the river of Volga. Changes in the discharge from the Volga do not effect the entire sea immediately. Therefore, the locations that are closer to the river experience fluctuations in water level sooner than the more distant locations. Consequently, it seems that point-wise analysis is more suitable for the investigation of the variations in the Caspian Sea's water level and the same may be said for other inland water source.

- Long-term in-situ daily tide-gauge observations in the Anzali port (1982-2006) show a non-linear trend in the Caspian Sea containing a periodic component with 12.5-years period.

- The LSSA of the SSH residuals time-series shows the presence of significant tidal frequencies that are aliased to other frequencies.

- The LSSA of the satellite orbital heights time-series indicates some significant frequencies, which are also present in the SSH power spectra.

- Applying the LSSA to a 5-year flow record of the Volga River observations indicates 5 major frequencies in addition to the annual and semi-annual frequencies. Studying the phase distribution of these frequencies shows that their influences on the Caspian Sea level are location-dependent.

- Annual, semi-annual and seasonal frequencies are clearly visible in the Caspian Sea. Moreover, there is a c.a. 0.0009 cpd frequency in both SSH and tide-gauge time-series. Interpretation of this frequency is still an open question.

Acknowledgement: The authors thank Dr. K. Fleming for his valuable comments that helped to considerably improve the original version of this article. M.A. Sharifi gratefully acknowledges the generous funding from the Deutscher Akademischer Austausch Dienst (DAAD) through award A/08/00069. J.L. Awange acknowledges the financial support of a Curtin Research Fellowship and the Alexander von Humboldt (Ludwig Leichhardt Memorial Fellowship) Foundation that supported his time at Curtin University and Karlsruhe Institute of Technology (KIT), respectively. E. Foorotan would like to thank Bonn University for the financial support.

References

Awange, J.L., Ogalo, L., Bae, K.H., Were, P., Omondi, P., Omute, P., & Omullo, M. (2008). Falling lake Victoria water levels: is climate a con-

tributing factor? pp. 1-20, DOI: 10.1007/s10584-008-9409-x.

Awange, J.L. & Ong'ang'a, O. (2006). Lake Victoria: ecology resource and environment. Springer, Berlin, 354 pp. ISBN-10: 3540325743.

Benada, J.R. (1997). TOPEX/POSEIDON Generation B (MGDR-B) User's Handbook, Version 2.0. Technical report, Physical Oceanography Distributed Active Archive Center (PODAAC), Jet Propulsion Laboratory, California Institute of Technology.

Bird, E.C.F. (2010). Iran-Caspian Sea coast (Springer Netherlands), pp. 861-866, DOI: http: //dx.doi.org/10.1007/978-1-4020-8639-7_149.

Birkett, C.M. (1995). The contribution of TOPEX/POSEIDON to the global monitoring of climatically sensitive lakes. Journal of Geophysical Research 100, pp. 25179-25204. DOI: 10.1029/95JC02125.

Birkett, C.M. (1994). Radara altimetry: new concept in monitoring lake level changes. EOS, 75, pp. 273-275. DOI: 10.1029/94EO00944.

Cartwright, D. (1993). Satellite altimetry in geodesy and oceanography: theory of ocean tides with application to altimetry, Springer Berlin / Heidelberg, pp. 100-141. DOI: http: //dx.doi.org/10.1007/BFb0117927.

Cazenave, A., Bonnefond, P., Dominh, K. & Schaeffer, P. (1997). Caspian Sea level from TOPEX/POSEIDON altimetry: Level now falling. Geophysical Research Letters 24 (8), pp. 881-884. DOI: http: //dx.doi.org/10.1029/97GL00809.

551 Cazenave, A., Schaeffer, P., Berge, M., Brossier, C., Dominh, K. & Gennero,
552 M.C. (1996). High-resolution mean sea surface computed with altimeter
553 data of ERS-1 (geodetic mission) and TOPEX/POSEIDON. Geophys J.
554 Int., 125, pp. 696-704. DOI: 10.1111/j.1365-246X.1996.tb06017.x.

555 Chatfield, C. (1989). The analysis of time series: an introduction (Chapman
556 and Hall), 352 pp. ISBN-10: 1584883170.

557 Craymer, M. (1998). The least squares spectrum, its inverse transform and
558 autocorrelation function: theory and some applications in Geodesy. PhD
559 thesis, University of Toronto, Canada.

560 Dumont, H.J. (1998). The Caspian Lake: history, biota, structure, and func-
561 tion. Limnnology and Oceanography 43, pp. 44-52. ISSN: 0024-3590.

562 Dumont, H.J., Tamara, A., Shiganova, U.N. (2004). Aquatic invasions in the
563 Black, Caspian, and Mediterranean Seas (Nato Science Series). Kluwer
564 Academic Publishers, 313 pp. ISBN-10: 140201869X.

565 Foster, G. (1996). Time series analysis by projection. I. statistical prop-
566 erties of Fourier analysis. Astronomical Journal 111, pp. 541-554. DOI:
567 10.1086/117805.

568 Georgievskiy, V.Y. (2001). A review and critical analysis of the
569 methods and results of the Caspian Sea level forecasts, devel-
570 oped for 5 to 10 and 20 to 100 years horizons. Technical re-
571 port, CEP. www.caspianenvironment.org/report_miscell2.htm (access
572 date: 20.05.2008).

573 Gil, E. & de Toro, C. (2005). Improving tide-gauge data processing: A
574 method involving tidal frequencies and inverted barometer effect. Com-
575 put. Geosci., 31, pp. 1048-1058. DOI: 10.1016/j.cageo.2005.02.006.

576 Golosov, V. & Belyaev, V. (2010). The Volga River basin
577 report. UNESCO International Sediment Initiative. Fac-
578 ulty of Geography, Lomonosov Moscow State University.
579 http://www.irtces.org/isi/isi_document/2010/ISI_Case_Study_Volga.pdf
580 (access date: 30.11.2010).

581 Hwang, C., Peng, M.F., Ning, J., Luo, J. & Sui, C.H. (2005). Lake level varia-
582 tions in China from TOPEX/Poseidon altimetry: data quality assessment
583 and links to precipitation and ENSO. Geophysical Journal International
584 161, pp. 1-16. DOI: 10.1111/j.1365-246X.2005.02518.x.

585 Ignatov, Ye.I.,Kaplin, P.A., Lukyanova S.A. & Solovieva G.D. (1993). Evolu-
586 tion of the Caspian Sea coasts under conditions of sea-level rise: model for
587 coastal change under Increasing "Greenhouse Effect". Journal of Coastal
588 Research 9 (1), pp. 104-111. ISSN: 0749-0208.

589 Kosarev, A.N. & Yablonskaya, E.A. (1994). The Caspian Sea (The Nether-
590 lands: SPB Academic Publishing), 260 pp. ISBN-10: 9051030886.

591 Kostianoy, A.G. & Lebedev, S.A. (2006). Satellite altimetry of the Caspian
592 Sea. 15 Years of Progress in Radar Altimetry Symposium, Venice Lido,
593 Italy, pp. 13-18 March 2006. http://www.iki.rssi.ru/earth/articles06/vol2-
594 113-120.pdf (access date: 30.11.2010).

595 Leontiev, O.K., Maev, E.G. & Rychagov, G.I. (1977). Geomorphology of the
596 Caspian Sea coasts and floor. Moscow: MGU, 208 pp. (in Russian).

597 Lyubushin, A.A., Gelder, P.H.A.J.M. & Bolgov, M.V. (2004). Spectral anal-
598 ysis of Caspian level variations. In Proceedings of the 23rd International
599 Conference on Off-shore Mechanics and Arctic Engineering, June 20-25,
600 Vancouver, British Columbia, Canada. pp. 108-110. ISBN: 90-805649-9-0.

601 Medina, C.E., Gomez-Enria, J., Alonsoa, J.J. & Villaresa, P. (2008).
602 Water level fluctuations derived from ENVISAT Radar Altimeter (RA-
603 2) and in-situ measurements in a subtropical waterbody: Lake Izabal
604 (Guatemala). Remote Sensing of Environment 112, pp. 3604-3617. DOI:
605 10.1016/j.rse.2008.05.001.

606 Minster, J.F., Brossier, C. & Rogel, P. (1995). Variation of the mean sea level
607 from TOPEX/POSEIDON data. J. Geophys Res 100, pp. 25153-25161.
608 DOI: 10.1029/95JC02304.

609 Nerem, R.S. (1995). Measuring global mean sea level variation using
610 TOPEX/POSEIDON altimeter data. J. Geophys Res 100, pp. 25135-
611 25151. DOI: 10.1029/95JC02303.

612 Nerem, R.S., Putney, B.H., and Marshall, J.A., Lerch, F.J., Pavlis, E.C.,
613 Klosko, S.M., Luthcke, S.B., Patel, G.B., Williamson, R.G. & Ze-
614 lensky, N.P. (1993). Expected orbit determination performance for the
615 TOPEX/Poseidon mission. Geoscience and Remote Sensing, IEEE Trans-
616 actions 31, pp. 333-354. DOI: 10.1109/36.214910.

Rodionov, S.N. (1994). Global and regional climate interaction: The Caspian Sea experience (Springer), pp. 256. ISBN-10: 0792327845.

Rubin, D.B. (2002). Statistical analysis with missing data (Wiley, New York), 408 pp. ISBN-10: 0471183865.

Shannon, C. (1984). Communication in the presence of noise. Proceedings of the IEEE, 72, pp. 1192-1201. DOI: 10.1109/PROC.1984.12998.

Steeves, R.R. (1981). A statistical test for significance of peaks in the least squares spectrum. In Collected Papers of the Geodetic Survey. Department of Energy, Mines and Resources, Surveys and Mapping, Ottawa. pp. 149-166.

von Storch, H., Woth, K. (2008). Storm surges: perspectives and options. Sustainability Science 3, pp. 33-43. DOI: 10.1007/s11625-008-0044-2.

Swenson, S. & Wahr J. (2007). Multi-sensor analysis of water storage variations of the Caspian Sea. Geophysical Research Letters 34, L16401, DOI: 10.1029/2007GL030733.

TDA (2002). Trans boundary diagnostic analysis for the Caspian Sea, The Caspian Sea environment programme 2002. http://www.caspianenvironment.org (access date: 31.10.2010).

Vanícêk , P. (1969). Approximate spectral analysis by Least-Squares Fit. Successive spectral analysis. Astrophysics and Space Science, 4, pp. 387-391. DOI: 10.1007/BF00651344.

638 Vanícêk, P & Krakiwsky, E. (1986). Geodesy the concepts (New York: Else-
639 vier science publishing). 697 pp. ISBN-10: 0444877770.

640 Vityazev, V. V. (1996). Time series analysis of unequally spaced data: In-
641 tercomparison between the Schuster periodogram and the LS-spectra. As-
642 tronomical and Astrophysical Transactions: The Journal of the Eurasian
643 Astronomical Society 11, pp. 139-158. DOI: 10.1080/10556799608205461.

644 Wang, Y. (2004). Ocean tide modeling in southern ocean. Technical report
645 471, Department of civil and Environmental Engineering and Geodetic
646 Science, The Ohio State University.

647 Wells, D., Vanícêk, P. & Pagiatakis, S. (1985). Least squares
648 spectral analysis revisited, Lecture notes. Department of Geodesy
649 and Geomatics Engineering, University of New Brunswick (UNB).
650 http//gge.unb.ca/Pubs/TR84.pdf (access date: 31.10.2010).

651 Wu, D. L., Hays, P. & Skinner, W. (1995). A least squares method for spectral
652 analysis of space-time series. Journal of the Atmospheric Sciences 52, pp.
653 3501-3511. DOI: 10.1175/1520-0469(1995)052<3501:ALSMFS>2.0.CO;2.

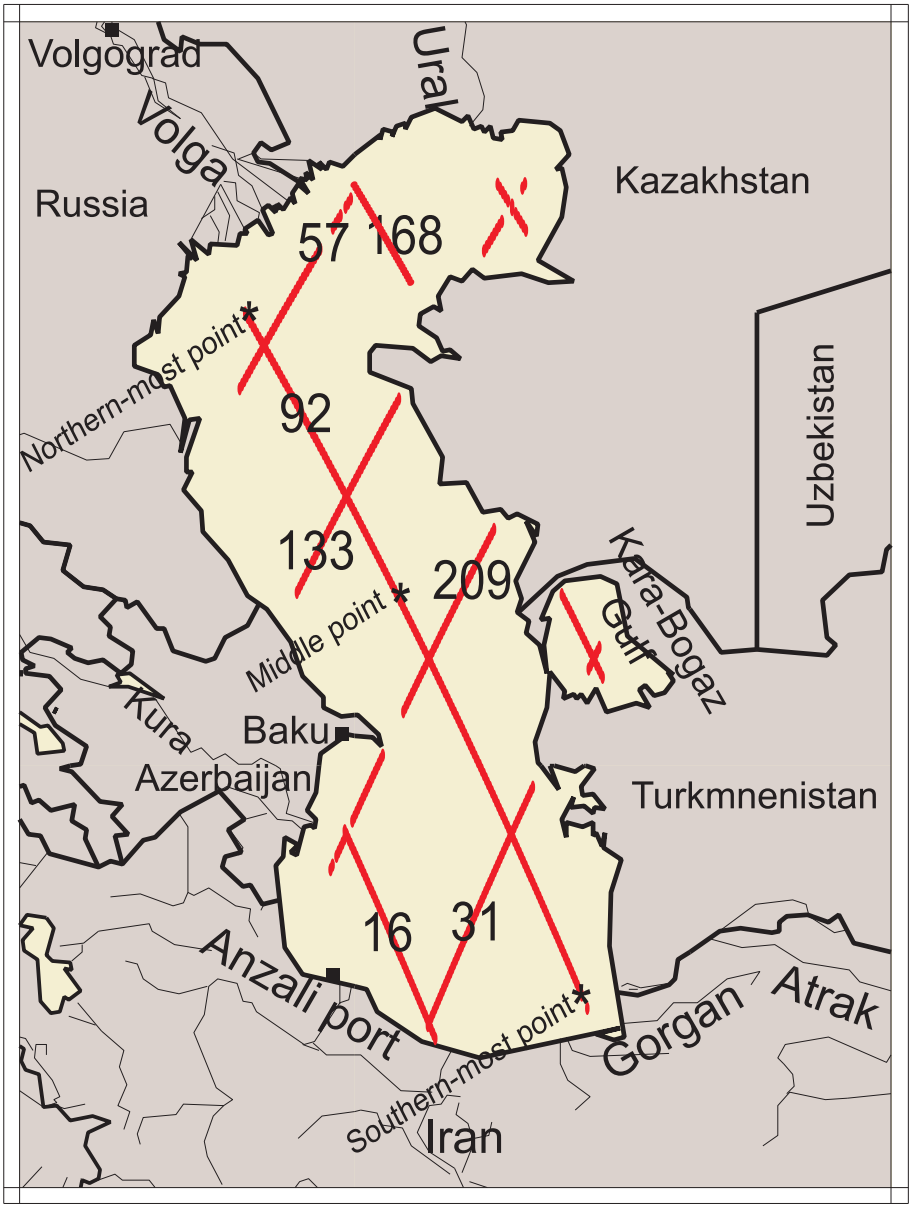

Figure 1: The Caspian Sea and its sorrounding regions. Figure shows the T/P's ground-tracks within the Caspian Sea.

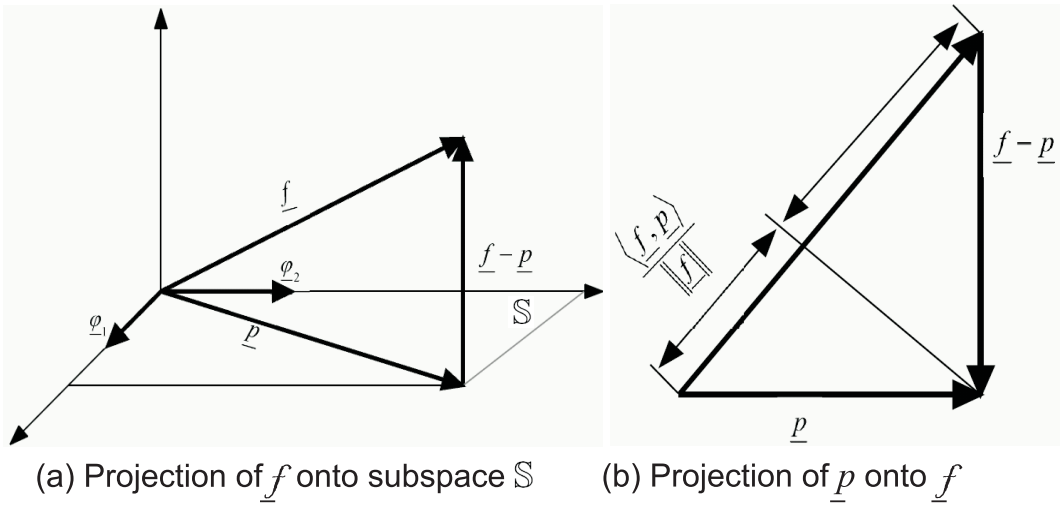

Figure 2: Geometrical explanation of the Least Squares Spectral Analysis (LSSA) (a) The projection of the observation vector ($\underline{\mathbf{f}}$) on to two orthogonal components $\underline{\phi_1}$, $\underline{\phi_2}$ (in our case, the orthogonal components are sine and cosine functions). The projection result is shown by vector $\underline{\mathbf{p}}$ which now belongs to the subspace $\mathbb{S}$. (b) The second projection of LSSA that leads to the computation of the power spectrum. Vector $\underline{\mathbf{p}}$ is projected back on to the observation vector $\underline{\mathbf{f}}$. The ratio of the length of this orthogonal projection to the length of observation vector $\underline{\mathbf{f}}$ gives the power value as (Eq 6) (Wells et al. (1985)).

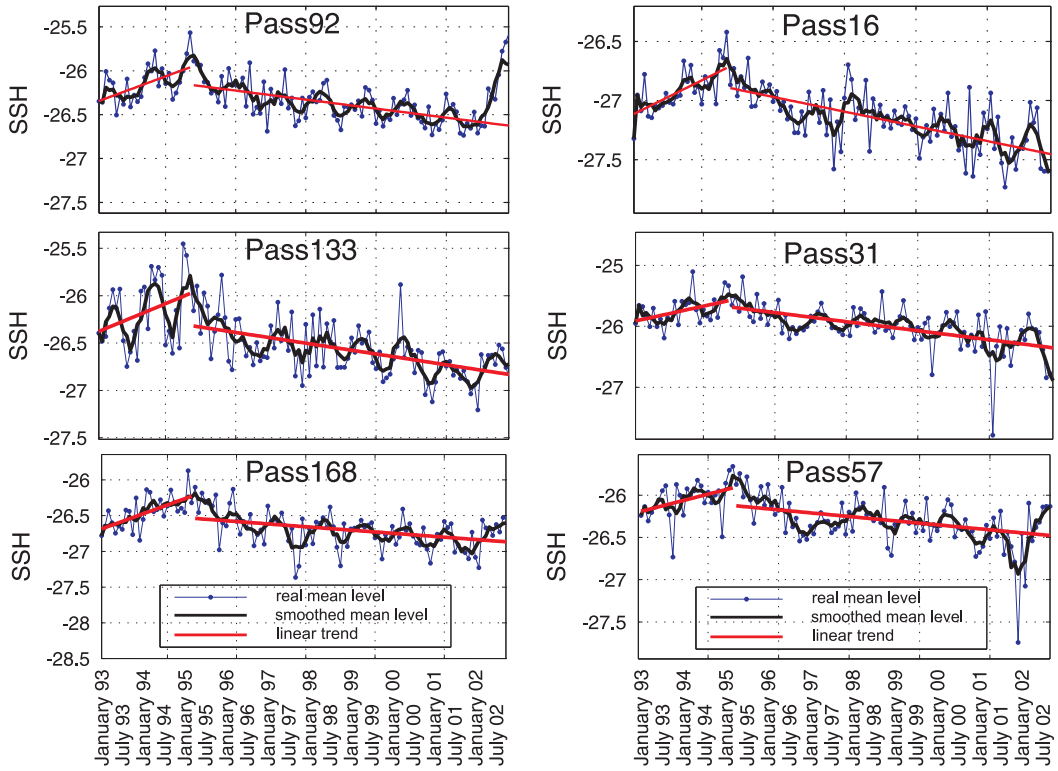

Figure 3: Monthly Caspian Sea water level variations as observed by T/P (see Fig. (1). The results are derived from the *pass-wise approach described in section 5.1 using 6 passes who had reliable observations within the 400 cycles.*

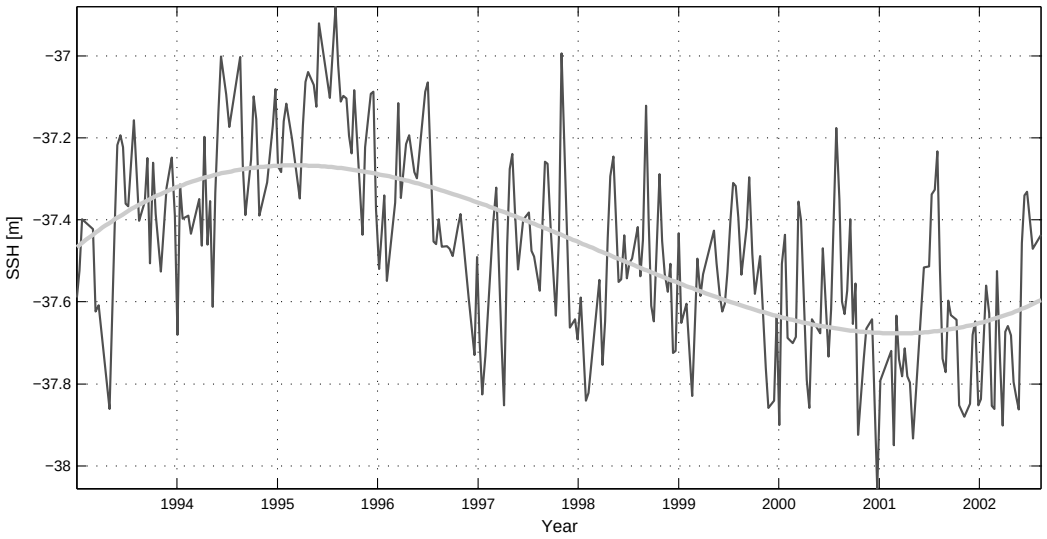

Figure 4: Point-wise SSH variations of a sample point in the middle Caspian Sea during 1993–2003 (see Fig. 1). The gray line shows the polynomial trend computed from tide gauge observations.

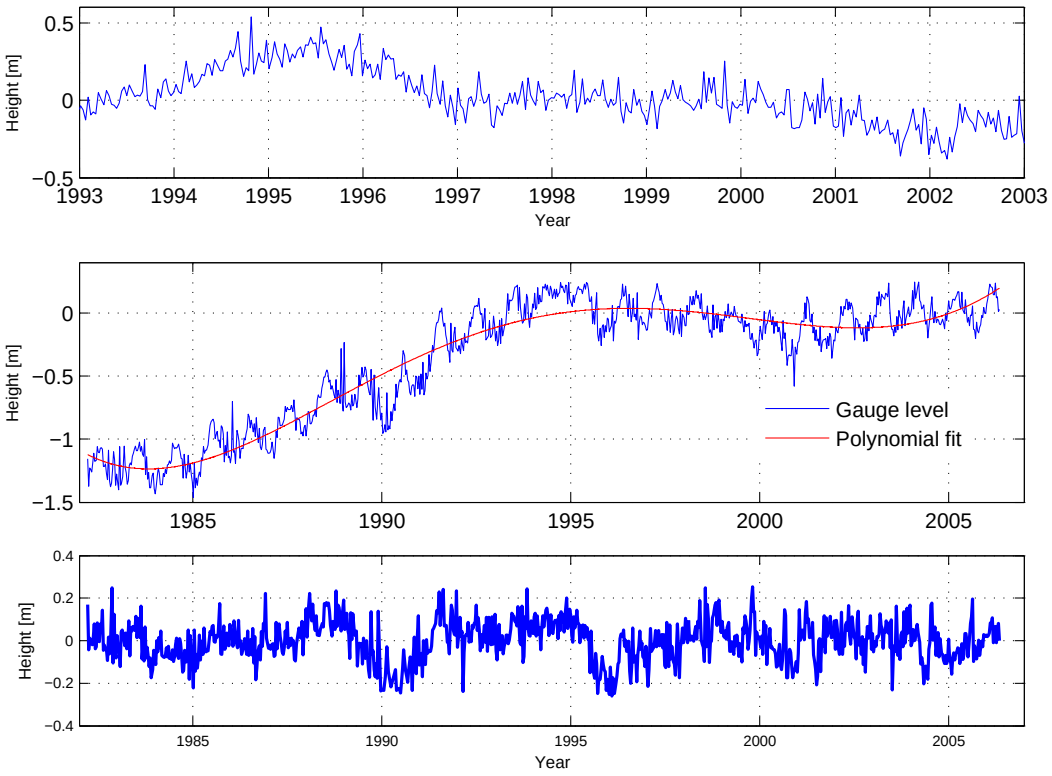

Figure 5: Anzali gauge records during 1993–2003 (top), 1982–2006 (middle), 1982–2006 (after detrending, in bottom)

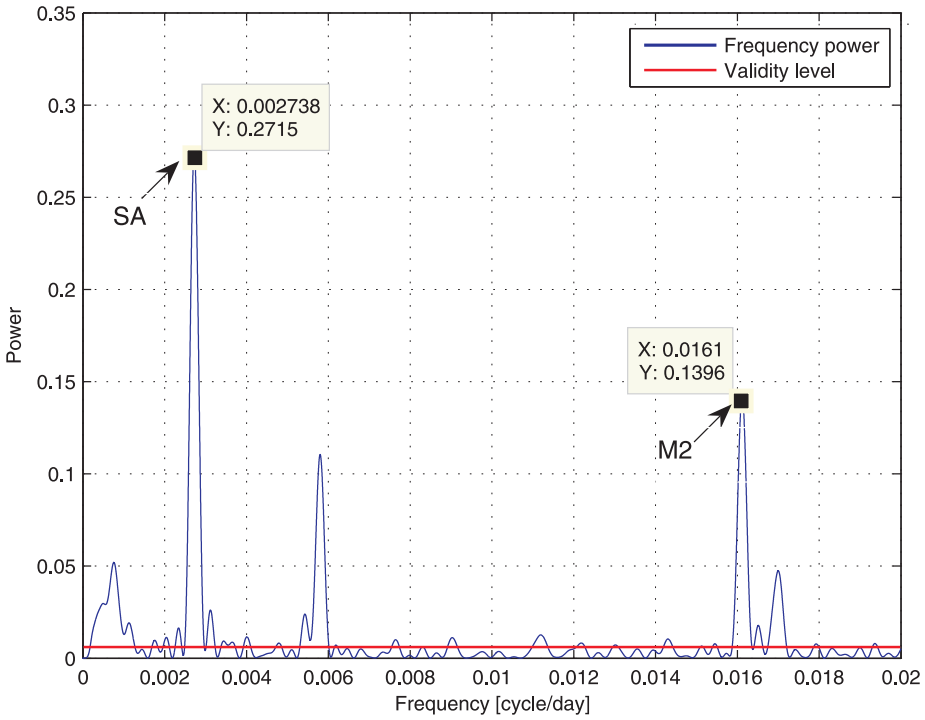

Figure 6: Power spectrum of the detrended SSH of the sample point's record (Fig. 4). In this figure $M2$ stands for lunar semidurnal frequency and SA is for the Sun annual frequency.

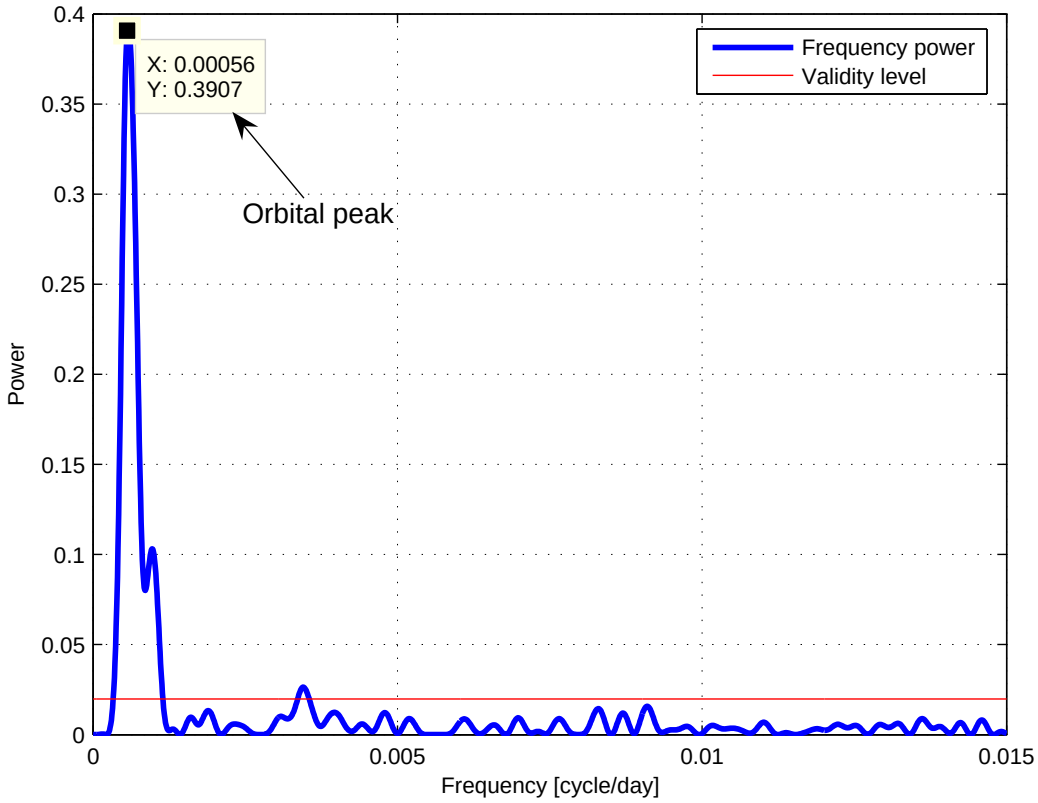

Figure 7: The sample point (Fig. 4) SSH spectrum after removing the tidal components

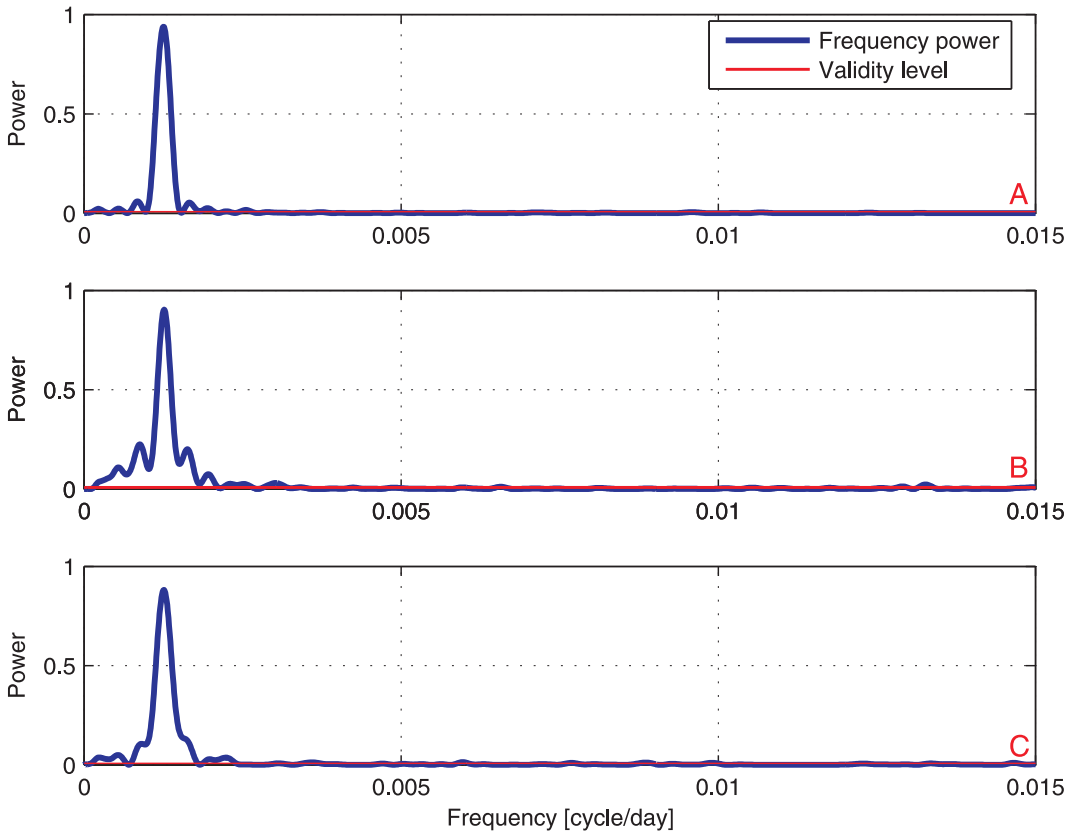

Figure 8: Power spectrum of satellite height time series at three different sample points above: A) the Caspian Sea, B) the lake Victoria and C) the Atlantic ocean. The spectra all shows a similar pattern.

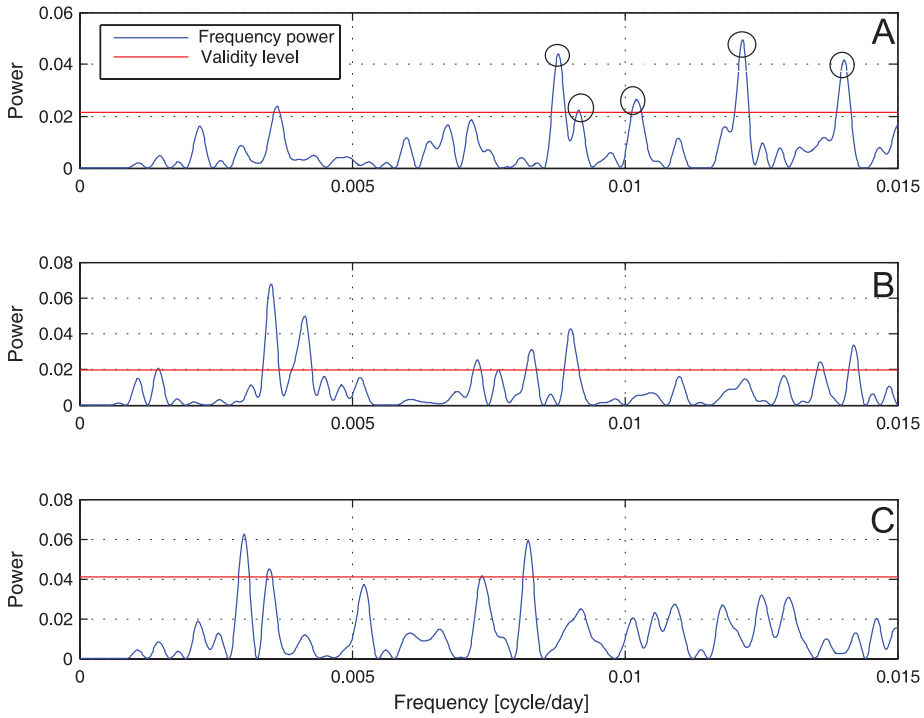

Figure 9: Power spectrum of three different points in the Caspian Sea, A) a sample point located near the Volga River entrance ($\phi = 44.864°$, $\lambda = 48.012°$), B) a point in the middle of the Caspian Sea ($\phi = 42.286°$, $\lambda = 50.164°$) and C) a point in the south of the Caspian Sea ($\phi = 37.594°$, $\lambda = 53.538°$).

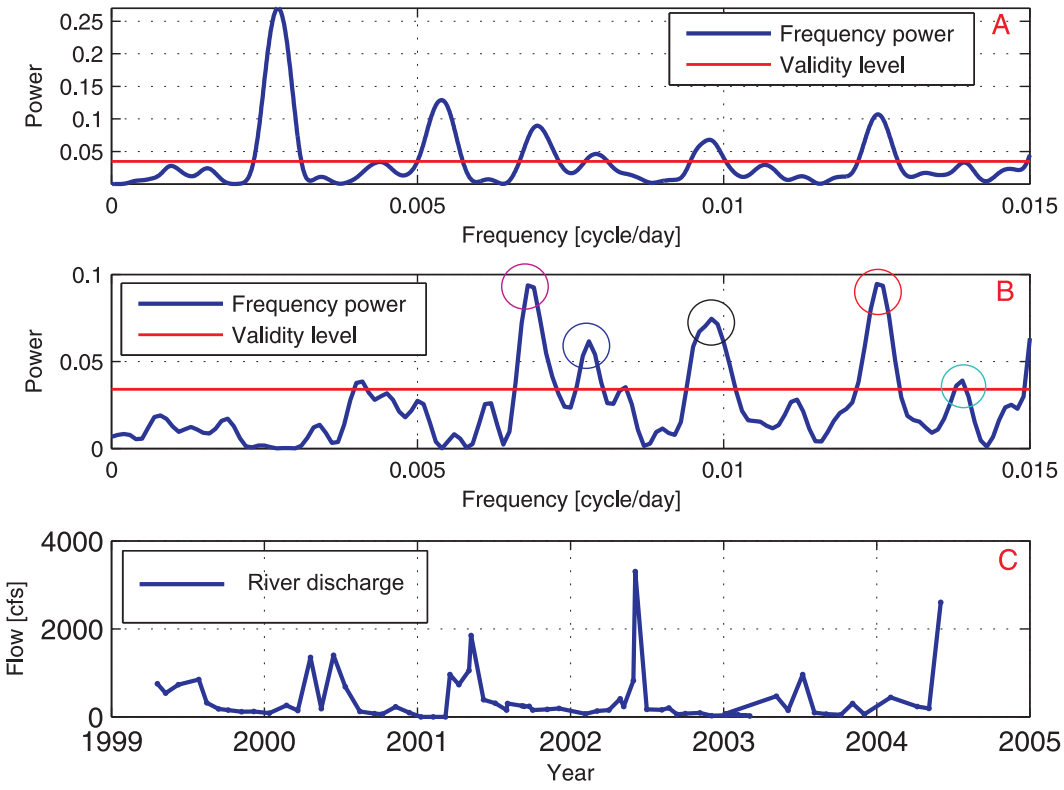

Figure 10: The Volga River's record during (1999-2005) A) Power spectrum of monthly Volga River discharge in cubic feet per second (cfs), B) Power spectrum of monthly Volga River flow without annual and semi-annual effects, C) Monthly discharge variations of the Volga River at the Volgagrad sampling site.

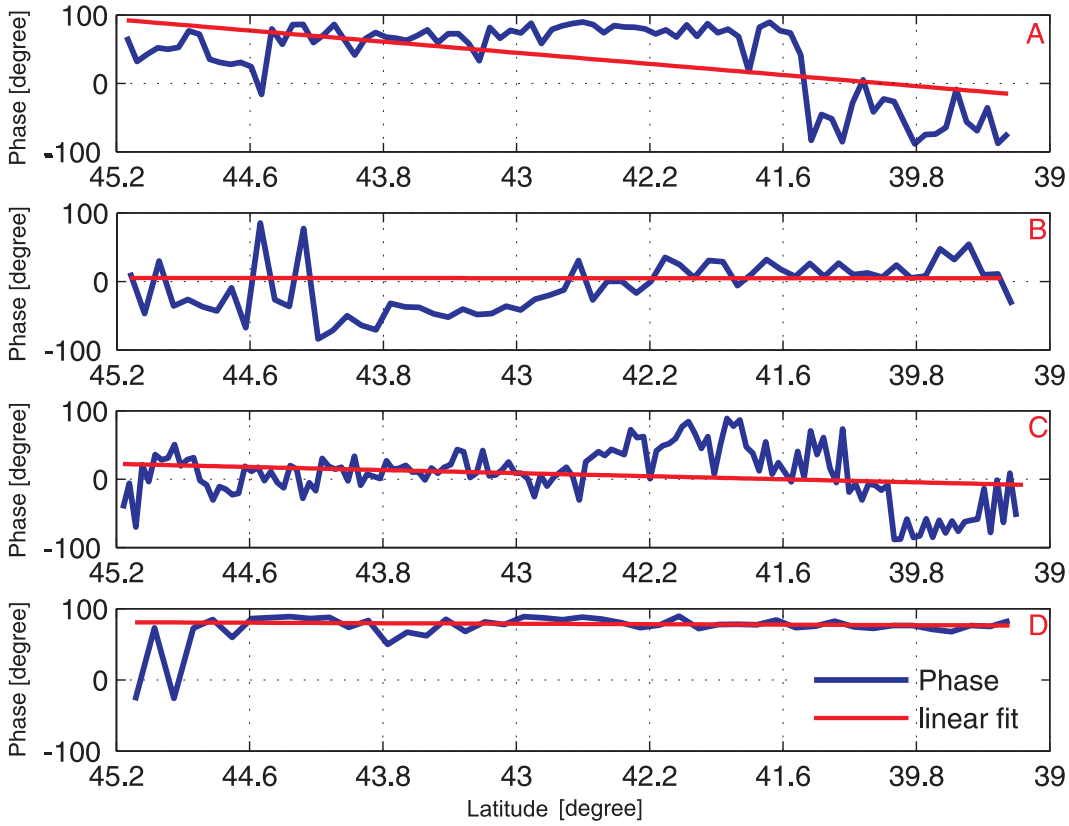

Figure 11: Effect of the Volga River on the Caspian Sea level fluctuations showing the southward phase variation of the Volga River discharge related to the: A) 0.0068 cpd, B) 0.0078 cpd, C) 0.0098 cpd and D) 0.0112 cpd frequencies.

Tables

Table 1:

Sign	Frequency (cpd)	Period (day)	Aliased Frequency (cpd)	Aliased Period (day)
SA	0.002738	365.260	0.002738	365.260
SSA	0.005476	182.621	0.005476	182.621
MSM	0.031435	31.812	0.031435	31.812
MM	0.036292	27.555	0.036292	27.555
MSF	0.067726	14.765	0.033125	30.189
MF	0.073202	13.661	0.027649	36.168
Q_1	0.893244	1.120	0.014417	69.365
O_1	0.929536	1.076	0.021875	45.714
P_1	0.997262	1.003	0.011250	88.891
S_1	1.000000	1.000	0.008512	117.485
K_1	1.002738	0.997	0.005774	17./192
O_2	1.859071	0.538	0.043750	22.857
N_2	1.895982	0.527	0.020191	49.528
M_2	1.932274	0.518	0.016101	62.107
S_2	2.000000	0.500	0.017024	58.742
K_2	2.005476	0.499	0.011548	86.596
M_3	2.898410	0.345	0.026274	38.061
M_4	3.864547	0.259	0.032202	31.054
S_4	4.000000	0.250	0.034047	29.371
M_6	5.796821	0.173	0.048303	20.702
S_6	6.000000	0.167	0.049780	20.088
M_8	7.729094	0.129	0.036447	27.437